Electrochemistry Communications 69 (2016) 46–49

Contents lists available at ScienceDirect

Electrochemistry Communications

journal homepage: www.elsevier.com/locate/elecom

Pseudocapacitive effect and Li^+ diffusion coefficient in three-dimensionally ordered macroporous vanadium oxide for energy storage

Zhongqiu Tong [a,b], Hongbo Xu [c], Guangqun Liu [d], Jiupeng Zhao [c], Yao Li [b,*]

[a] College of Materials and Metallurgical Engineering, Guizhou Institute of Technology, Guiyang 550003, China
[b] Center for Composite Materials and Structure, Harbin Institute of Technology, Harbin 150001, China
[c] School of Chemical Engineering and Technology, Harbin Institute of Technology, 150001 Harbin, China
[d] College of Science, Guizhou Institute of Technology, Guiyang 550003, China

ARTICLE INFO

Article history:
Received 17 May 2016
Received in revised form 21 May 2016
Accepted 22 May 2016
Available online 24 May 2016

Keywords:
Three-dimensionally ordered macroporous structure
Pseudocapacitive effect
Li-ion diffusion coefficient
High rate capability
Vanadium oxide

ABSTRACT

In order to act as extrinsic pseudocapacitor materials, nanoscale vanadium oxides are required to simultaneously exhibit a capacitance-based high power density and an intercalation-based high energy density. We have fabricated a three-dimensionally ordered macroporous (3DOM) structure with a wall thickness of 14 nm that fulfills the above requirements. The 3DOM vanadium oxide film exhibits high rate performance with 355 F g^{-1} at 0.5 A g^{-1} and 125 F g^{-1} at 15 A g^{-1}. The enhanced pesudocapacitive effect and Li-ion diffusion coefficient based on the 3DOM nanostructure, also contributes to the high rate capability of vanadia, which can be confirmed by cyclic voltammetry and chronoamperometry.

1. Introduction

Vanadium oxides have been widely studied as electrochemical energy storage materials for supercapacitors and Li-ion batteries [1–7] because of their ability to undergo redox intercalation [6,8–10] and the various available oxidation states of vanadium (V–II) [10]. However, their small Li-ion diffusion coefficient and electrical conductivity [11–15] cause the intercalation process to be slow, seriously limiting their energy storage performance [16]. Nanostructured vanadium oxides can provide shortened Li-ion diffusion distances and increased surface areas, leading to efficient Li-ion intercalation and, therefore, to high energy density [17]. Another significant phenomenon that occurs with nanostructuring is the pseudocapacitive effect, originating from the fast faradaic processes occurring at the materials' surface, which can generate high power density [6,18–20]. Nanostructuring is of special significance for vanadium oxides because they are extrinsic pseudocapacitor materials [1,3,5,6,21–25]. The pseudocapacitance of nanostructured vanadia depends strongly on their contact area with the electrolyte. For example, aerogels exhibit almost perfect capacitive cyclic voltammetry (CV) curves [5], while electrospun nanorods exhibit CV curves with sharp and well-separated redox peaks [2].

Among the various nanostructures available, the three-dimensionally ordered macroporous (3DOM) structure is an important nanoarchitecture for Li-ion storage materials [26–30]. Its bicontinuous structure provides intercontinuous voids for good electrolyte penetration, and continuous thin walls for effective electron transport and Li-ion intercalation. Typically, 3DOM structures are prepared from face-centered-cubic colloidal crystals. The sphere packing factor of 74% in colloidal crystal produces 3DOM materials with a similar porosity and a high surface area [26]. Furthermore, employing small diameter spheres results in 3DOM materials with thin wall structures that may exhibit pseudocapacitive behavior [1,5,6,21–25].

Herein, we have prepared 3DOM vanadium oxide films by electrodeposition within colloidal crystals. The films exhibit a significantly enhanced rate capability. Besides the typical advantages nanostructuring provides, CV and chronoamperometry have revealed that the observed improved performance is also the result of pseudocapacitive effect and improved Li-ion diffusion coefficient.

2. Experimental

Polystyrene colloidal crystals with a sphere diameter of 165 or 480 nm on indium-doped tin oxide substrates were grown by a controlled vertical drying method [31,32]. Anodic deposition of vanadia within the colloidal crystals was performed at 2 V versus Ag/AgCl from a 1:1 mixture of deionized water and ethanol containing $VOSO_4$ (0.25 M). After removing the template with toluene and drying at 120 °C for 6 h, 3DOM vanadia films were obtained. The 3DOM vanadia samples obtained from colloidal crystals with sphere diameter values

* Corresponding author.
E-mail address: yaoli@hit.eu.cn (Y. Li).

http://dx.doi.org/10.1016/j.elecom.2016.05.017
1388-2481/

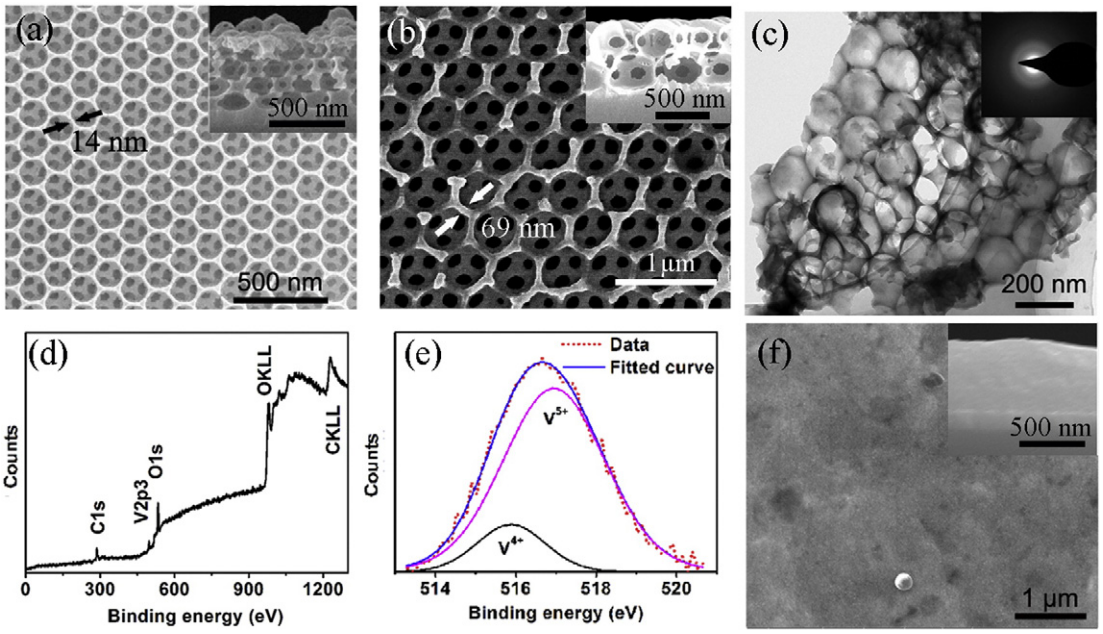

Fig. 1. SEM images of (a) SD-165 nm and (b) SD-480 nm (side view in the inset). TEM image of (c) SD-165 nm (SAED pattern in the inset). (d) Wide-range XPS spectrum, and (e) $V2p_{3/2}$ core peak spectra of SD-165 nm. (f) SEM images of the compact vanadia film (side view in the inset).

of 165 and 480 nm were denoted as SD-165 nm and SD-480 nm, respectively. For comparison, template-free vanadia films were also prepared. The mass loading of SD-165 nm, SD-480 nm, and template-free film were ca. 0.42, 0.55, and 1.57 mg cm^{-2}, respectively.

Scanning electron microscopy (SEM) images were taken with a FEI Helios Nanolab 600i instrument. Transmission electron microscopy (TEM) images and selected-area electron diffraction (SAED) patterns were recorded on a FEI Tecnai G2F30 instrument. X-ray photoelectron spectroscopy (XPS) analysis was conducted on a PHI 5700 ESCA system. The electrochemical properties were evaluated using a nitrogen-filled three-electrode cell with an electrochemical analyzer (CHI 660D) in 1M $LiClO_4$–propylene carbonate. A Ag/AgCl electrode was used as the reference electrode and a platinum plate was employed as the counter electrode. A Luggin capillary connected by a salt bridge was used to minimize *iR*-drop errors and to prevent contamination of the cell electrolyte.

3. Results and discussion

Due to the 3D ordered structure of the colloidal crystals, the SD-165 nm and SD-480 nm samples display honeycomb-like structures throughout their entire volume, with nanoscale walls with thickness of about 14 and 69 nm, respectively (Fig. 1a and b). Although powerful ultrasonication during the TEM-sample preparation partly destroyed its structure, the 3DOM nanostructure of SD-165 nm is still clearly observed (Fig. 1c). The presence of only amorphous rings in the SAED pattern indicates that the as-deposited vanadia is amorphous. The XPS results of the 3DOM vanadia demonstrate its high purity and the presence of a mixture of V^{4+} (515.8 eV) and V^{5+} (516.9 eV) species (Fig. 1d and e) [33]. The template-free vanadia film exhibits a compact nature (Fig. 1f).

Fig. 2a, b, and c shows, respectively, the galvanostatic discharge/charge performance of SD-165 nm, SD-480 nm, and the compact films at 0.5, 1, 2, 5, 10, and 15 A g^{-1}. These films show featureless and symmetric discharge/charge curves, similar to the curves of other amorphous and nanocrystalline vanadia species [1,6,21–25], indicating that they are suitable materials for supercapacitors [6]. The 3DOM films exhibit a much higher specific capacitance (C_s) and rate capability than the compact film, and the 3DOM film with smaller pores (SD-165 nm) shows higher C_s values (Fig. 2d). At 0.5 A g^{-1}, the C_s value of SD-165 nm was calculated to be 355 F g^{-1}, higher than that of SD-480 nm and the compact film (240 and 187 F g^{-1}, respectively). When the current density reached a high value of 15 A g^{-1}, SD-165 nm still maintained a high C_s value of 125 F g^{-1}, whereas values of merely 74 and 22 F g^{-1} were obtained for SD-480 nm and the compact film, respectively. SD-165 nm exhibits superior charge storage performance compared to many other high-surface-area vanadia, such as nanosheets (314 F g^{-1} at 0.5 A g^{-1}), interconnected nanoporous networks (304 F g^{-1} at 0.1 A g^{-1}), and starfruit-like nanoparticles (216 F g^{-1} at 1 A g^{-1}) [25,34–39].

Besides the common advantages of nanostructures, such as large surface area and short Li-ion diffusion paths [40], the absence of plateau

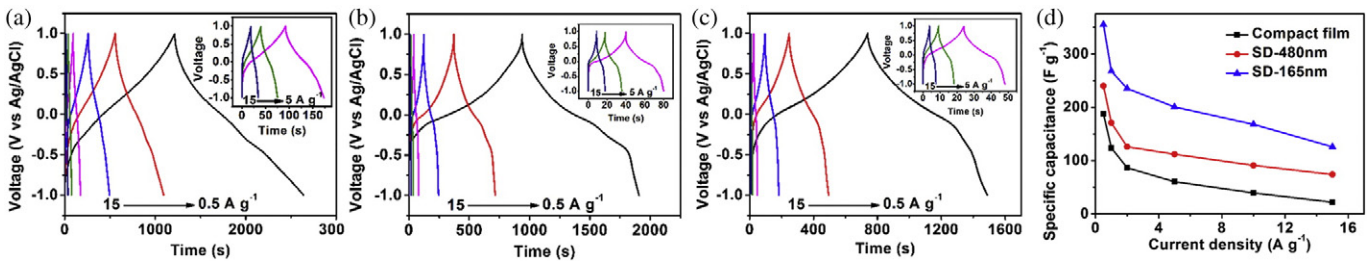

Fig. 2. Galvanostatic charge/discharge curves of (a) SD-165 nm, (b) SD-480 nm, (c) the compact film, and (d) variation of the specific capacitance with the current density for the three vanadia films.

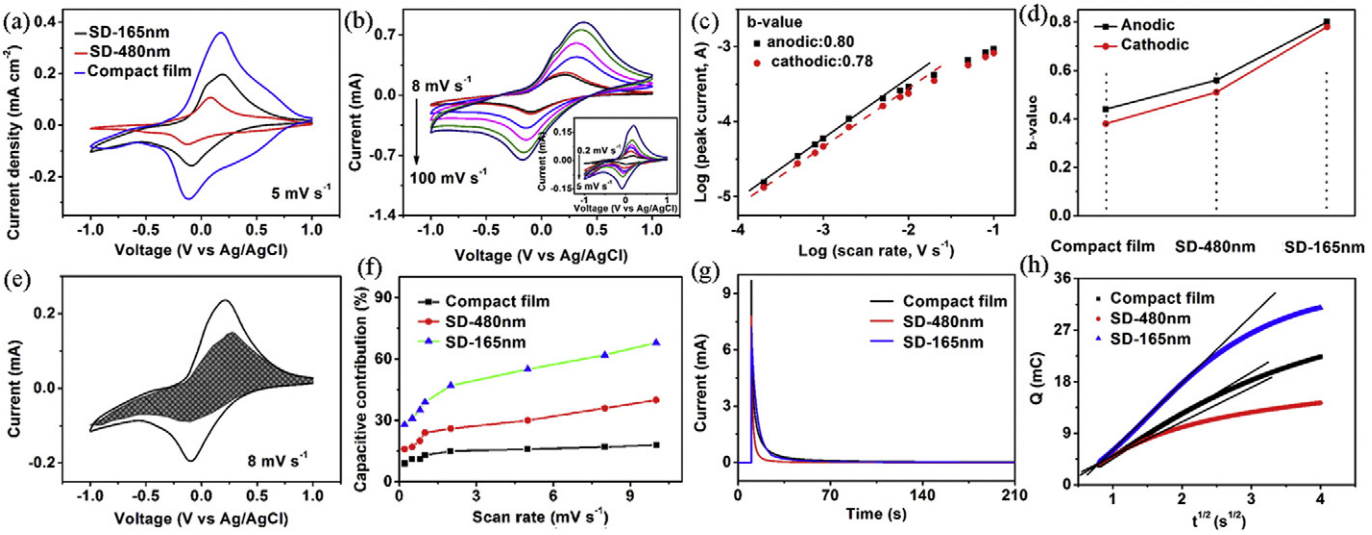

Fig. 3. (a) CV curves of SD-165 nm, SD-480 nm and the compact film at 5 mV s^{-1}. (b) CV curves of SD-165 nm at various scan rates and (c) the corresponding log(i) vs. log(v) plots. (d) Summarized b-values for the three vanadia films. (e) Separation of the capacitive (shaded) and diffusion currents in SD-165 nm at 8 mV s^{-1}. (f) Capacitive contribution ratio versus scan rate of the three vanadia films. (g) Chronocoulometric current response curves of the three vanadia films from 1 V to 0 V, and (h) the corresponding Q vs. $t^{1/2}$ plots.

region (indicating phase transformation-based Li-ion intercalation processes) in the charge/discharge curves of SD-165 nm indicates the possible existence of an enhanced pseudocapacitive effect related to the high rate performance observed for this structure [6,18,19]. CV analysis was conducted in order to investigate the influence of the 3DOM structure on the electrochemical behavior of as-deposited vanadia. The similarity among the CV profiles of these three films demonstrates their similar chemical composition (Fig. 3a). Assuming that the redox peak current (i) obeys a power–law relationship to the scan rate (v) leads to the relation $i = av^b$ [18,20], where a and b are adjustable values. When the value of b is 0.5, the current response is diffusion-controlled (intercalative), whereas a value of 1 indicates the current is surface-controlled (capacitive). Fig. 3b and c present the CV behavior of SD-165 nm at different scan rate, from 0.2 to 100 mV s^{-1}, and the corresponding plots of log(i) vs. log(v), respectively. Both the anodic and cathodic peaks of SD-165 nm exhibit a good log(i)–log(v) linear relation between 0.2 and 5 mV s^{-1}, and the calculated b-values are 0.80 and 0.78, respectively, confirming an enhancement of the pseudocapacitive effect and a high pseudocapacitive energy storage contribution. In contrast, SD-480 nm exhibits values of b of 0.56 and 0.51 for the anodic and cathodic peaks, respectively, and much smaller b-values of 0.44 and 0.38 were found for the compact film (Fig. 3d). The high b-values of SD-165 nm arise from enhanced surface redox reactions and significantly shortened Li-ion diffusion distances, probably even leading to the suppression of phase transformations [6,18,19]. Furthermore, for a specific CV scanning rate, v, the measured current, i, at a fixed potential, V, can be quantitatively separated into capacitive (k_1v) and diffusion-controlled ($k_1v^{1/2}$) responses according to $i(V) = k_1v + k_1v^{1/2}$ [6]. By determining k_1 and k_2, one can distinguish between Li-ion storage arising from intercalation and energy storage from capacitance. As shown in Fig. 3e, the diffusion-controlled charge of SD-165 nm is mainly generated around the peak voltage at 8 mV s^{-1}. The SD-165 nm sample shows a higher capacitive contribution than that of SD-480 nm and the compact film (Fig. 3f). For instance, 28% of the total charge is capacitive at 0.2 mV s^{-1} in SD-165 nm, whereas the capacitive contribution of SD-480 nm and the compact film is only 16% and 10%, respectively. At 10 mV s^{-1}, the capacitive contribution of SD-165 nm increases up to 68%, much higher than that of SD-480 nm (40%) and the compact film (18%). The high b-values and capacitive contribution of SD-165 nm are related to the film's high rate capability. This nanoscale-dependent electrochemical behavior confirms that vanadia is an extrinsic pseudocapacitor material [2,5,6].

Furthermore, the b-values of the SD-165 nm are far from 1, implying that a Li-ion intercalation also occurs. To further investigate the influence of the 3DOM structure on the Li-ion intercalation kinetics in vanadia, the Li-ion diffusion coefficient (D_{Li}) was evaluated by a chronocoulometric method through the equation: $Q = 2n^{-1/2}FAD_{Li}^{1/2}C_0t^{1/2} + Q_{dl} + nF\Gamma$ [13,31], where Q is the integrated charge, n is the number of electrons transferred in redox reactions, A is the electrode area, D_{Li} is the Li^+ chemical diffusion coefficient, C_0 is the Li^+ surface concentration, Q_{dl} is the double-layer charge, F represent faraday constant, and Γ is the concentration of adsorbed species during the faradic reaction. Fig. 3g and h shows the current response curves of the three films when the voltage was switched from 1 V to 0 V, and the corresponding plots of Q vs. $t^{1/2}$. The data show that the D_{Li} value of SD-165 nm is 2.13×10^{-10} cm^2 s^{-1}, higher than that of SD-480 nm (7.54×10^{-11} cm^2 s^{-1}) and the compact film (8.62×10^{-12} cm^2 s^{-1}). The improved D_{Li} value of the SD-165 nm film can be attributed to 3DOM-based structural advantages, that is, to a decreased electrode polarization, rough surface, and three-dimensional electron and Li-ion transport [13,31]. We believe that the improved D_{Li} value also influences positively the Li-ion storage performance of the SD-165 nm film, since a higher D_{Li} value can result in accelerated Li-ion intercalation, thus enabling more vanadium ions to take part in the redox reaction.

4. Conclusions

This study describes how the pseudocapacitive effect and Li^+ diffusion coefficient in 3DOM structures are two important factors that lead to superior energy rate performance of vanadia in an organic electrolyte. Due to the above features, the SD-165 nm vanadia film shows a high rate capability with a C_s of 355 F g^{-1} at 0.5 A g^{-1} and 125 F g^{-1} at 15 A g^{-1}, much higher than that of many other nanostructured vanadia electrodes. The present results are significant toward the applicability of 3DOM structures in energy storage, and the high Li-ion storage performance of this SD-165 nm vanadia film electrode makes it a promising candidate for electrochemical energy storage devices.

Acknowledgment

We thank National Natural Science Foundation of China (Nos. 51572058, 91216123, 51174063, 51502057).

References

[1] M. Sathiya, A.S. Prakash, K. Ramesha, J.M. Tarascon, A.K. Shukla, V_2O_5-anchored carbon nanotubes for enhanced electrochemical energy storage, J. Am. Chem. Soc. 133 (2011) 16291–16299.

[2] L. Mai, L. Xu, C. Han, X. Xu, Y. Luo, S. Zhao, Y. Zhao, Electrospun ultralong hierarchical vanadium oxide nanowires with high performance for lithium ion batteries, Nano Lett. 10 (2010) 4750–4755.

[3] D. McNulty, D.N. Buckley, C. O'Dwyer, Comparative electrochemical charge storage properties of bulk and nanoscale vanadium oxide electrodes, J. Solid State Electrochem. http://dx.doi.org/10.1007/s10008-016-3154-2.

[4] A. Pan, H. Wu, L. Yu, X.W. Lou, Template-free synthesis of VO_2 hollow microspheres with various interiors and their conversion into V_2O_5 for lithium-ion batteries, Angew. Chem. Int. Ed. 125 (2013) 2282–2286.

[5] E. Armstrong, D. McNulty, H. Geaney, C. O'Dwyer, Electrodeposited structurally stable V_2O_5 inverse opal networks as high performance thin film lithium batteries, ACS Appl. Mater. Interfaces 7 (2015) 27006–27015.

[6] V. Augustyn, P. Simon, B. Dunn, Pseudocapacitive oxide materials for high-rate electrochemical energy storage, Energy Environ. Sci. 7 (2014) 1597–1614.

[7] F. Wang, S. Xiao, Y. Hou, C. Hu, L. Liu, Y. Wu, Electrode materials for aqueous asymmetric supercapacitors, RSC Adv. 3 (2013) 13059–13084.

[8] P. Novák, W. Scheifele, F. Joho, O. Haas, Electrochemical insertion of magnesium into hydrated vanadium bronzes, J. Electrochem. Soc. 142 (1995) 2544–2550.

[9] Q. Wei, J. Liu, W. Feng, J. Sheng, X. Tian, L. He, Q. An, L. Mai, Hydrated vanadium pentoxide with superior sodium storage capacity, J. Mater. Chem. A 3 (2015) 8070–8075.

[10] Z. Tong, N. Li, H. Lv, Y. Tian, H. Qu, X. Zhang, J. Zhao, Y. Li, Annealing synthesis of coralline V_2O_5 nanorod architecture for multicolor energy-efficient electrochromic device, Sol. Energy Mater. Sol. Cells 146 (2016) 135–143.

[11] S. Yang, Y. Gong, Z. Liu, L. Zhan, D.P. Hashim, L. Ma, R. Vajtai, P.M. Ajayan, Bottom-up approach toward single-crystalline VO_2–graphene ribbons as cathodes for ultrafast lithium storage, Nano Lett. 13 (2013) 1596–1601.

[12] Z. Tong, H. Lv, X. Zhang, H. Yang, Y. Tian, N. Li, J. Zhao, Y. Li, Novel morphology changes from 3D ordered macroporous structure to V_2O_5 nanofiber grassland and its application in electrochromism, Sci. Rep. 5 (2015) 16864.

[13] Z. Tong, J. Hao, K. Zhang, J. Zhao, B. Su, Y. Li, Improved electrochromic performance and lithium diffusion coefficient in three-dimensionally ordered macroporous V_2O_5 films, J. Mater. Chem. C 2 (2014) 3651–3658.

[14] G. Stefanovich, A. Pergament, D. Stefanovich, Electrical switching and Mott transition in VO_2, J. Phys. Condens. Matter 12 (2000) 8837–8845.

[15] C. Sanchez, R. Morineau, J. Livage, Electrical conductivity of amorphous V_2O_5, Phys. Status Solidi A 76 (1983) 661–666.

[16] M. Benmoussa, E. Ibnouelghazi, A. Bennouna, E.L. Ameziane, Structural, electrical and optical properties of sputtered vanadium pentoxide thin films, Thin Solid Films 265 (1995) 22–28.

[17] P. Poizot, S. Laruelle, S. Grugeon, L. Dupont, J.-M. Tarascon, Nano-sized transition-metal oxides as negative-electrode materials for lithium-ion batteries, Nature 407 (2000) 496–499.

[18] P. Simon, Y. Gogotsi, B. Dunn, Where do batteries end and supercapacitors begin? Science 343 (2014) 1210–1211.

[19] T. Brousse, D. Bélanger, J.W. Long, To be or not to be pseudocapacitive? J. Electrochem. Soc. 162 (2010) A5185–A5189.

[20] V. Augustyn, J. Come, M.A. Lowe, J. Kim, P. Taberna, S.H. Tolbert, H.D. Abruña, P. Simon, B. Dunn, High-rate electrochemical energy storage through Li^+ intercalation pseudocapacitance, Nat. Mater. 12 (2013) 518–522.

[21] J. Livage, Sol–gel chemistry and electrochemical properties of vanadium oxide gels, Solid State Ionics 86-88 (1996) 935–942.

[22] Z. Chen, V. Augustyn, X. Jia, Q. Xiao, B. Dunn, Y. Lu, High-performance sodium-ion pseudocapacitors based on hierarchically porous nanowire composites, ACS Nano 6 (2012) 4319–4327.

[23] I.-H. Kim, J.-H. Kim, B.-W. Cho, K.-B. Kim, Pseudocapacitive properties of electrochemically prepared vanadium oxide on carbon nanotube film substrate, J. Electrochem. Soc. 153 (2006) A1451–A1458.

[24] S. Boukhalfa, K. Evanoff, G. Yushin, Atomic layer deposition of vanadium oxide on carbon nanotubes for high-power supercapacitor electrodes, Energy Environ. Sci. 5 (2012) 6872–6879.

[25] G. Wee, H. Soh, Y. Cheah, S. Mhaisalkar, M. Srinivasan, Synthesis and electrochemical properties of electrospun V_2O_5 nanofibers as supercapacitor electrodes, J. Mater. Chem. 20 (2010) 6720–6725.

[26] J.W. Long, B. Dunn, D.R. Rolison, H.S. White, Three-dimensional battery architectures, Chem. Rev. 104 (2004) 4463–4492.

[27] A. Stein, B.E. Wilson, S.G. Rudisill, Design and functionality of colloidal-crystal-templated materials—chemical applications of inverse opals, Chem. Soc. Rev. 42 (2013) 2763–2803.

[28] E.M. Sorensen, S.J. Barry, H. Jung, J.M. Rondinelli, J.T. Vaughey, K.R. Poeppelmeier, Three-dimensionally ordered macroporous $Li_4Ti_5O_{12}$: effect of wall structure on electrochemical properties, Chem. Mater. 18 (2006) 482–489.

[29] H. Yan, S. Sokolov, J.C. Lytle, A. Stein, F. Zhang, W.H. Smyrl, Colloidal-crystal-templated synthesis of ordered macroporous electrode materials for lithium secondary batteries, J. Electrochem. Soc. 150 (2003) A1102–A1107.

[30] H. Kim, M. Kim, J. Cho, Unique structural changes of three-dimensionally ordered macroporous TiO_2 electrode materials during electrochemical cycling, Adv. Energy Mater. 2 (2012) 1425–1432.

[31] Z. Tong, H. Yang, L. Na, H. Qu, X. Zhang, J. Zhao, Y. Li, Versatile displays based on a 3-dimensionally ordered macroporous vanadium oxide film for advanced electrochromic devices, J. Mater. Chem. C 3 (2015) 3159–3166.

[32] Z. Tong, X. Zhang, H. Lv, N. Li, H. Qu, J. Zhao, Y. Li, X. Liu, From amorphous macroporous film to 3D crystalline nanorod architecture: a new approach to obtain high-performance V_2O_5 electrochromism, Adv. Mater. Interfaces 2 (2015) 1500230.

[33] G. Silversmit, D. Depla, H. Poelman, G.B. Marin, R.D. Gryse, Determination of the V2p XPS binding energies for different vanadium oxidation states (V^{5+} to V^{0+}), J. Electron Spectrosc. Relat. Phenom. 135 (2004) 167–175.

[34] J. Zhu, L. Cao, Y. Wu, Y. Gong, Z. Liu, H.E. Hoster, Y. Zhang, S. Zhang, S. Yang, Q. Yan, P.M. Ajayan, R. Vajtai, Building 3D structures of vanadium pentoxide nanosheets and application as electrodes in supercapacitors, Nano Lett. 13 (2013) 5408–5413.

[35] J.S. Bonso, A. Rahy, S.D. Perera, N. Nour, O. Seitz, Y.J. Chabal, K.J. Balkus, J.P. Ferraris, D.J. Yang, Exfoliated graphite nanoplatelets–V_2O_5 nanotube composite electrodes for supercapacitors, J. Power Sources 203 (2012) 227–232.

[36] S.D. Perera, B. Patel, N. Nijem, K. Roodenko, O. Seitz, J.P. Ferraris, Y.J. Chabal, K.J. Balkus Jr., Vanadium oxide nanowire–carbon nanotube binder-free flexible electrodes for supercapacitors, Adv. Energy Mater. 1 (2011) 936–945.

[37] B. Kim, C. Kim, K. Yang, A. Rahy, D.J. Yang, Electrospun vanadium pentoxide/carbon nanofiber composites for supercapacitor electrodes, Electrochim. Acta 83 (2012) 335–340.

[38] B. Saravanakumar, K.K. Purushothaman, G. Muralidharan, Interconnected V_2O_5 nanoporous network for high-performance supercapacitors, ACS Appl. Mater. Interfaces 4 (2012) 4484–4490.

[39] J. Shao, X.Y. Li, Q.T. Qu, H.G. Zheng, One-step hydrothermal synthesis of hexangular starfruit-like vanadium oxide for high power aqueous supercapacitors, J. Power Sources 219 (2012) 253–257.

[40] Z.Q. Tong, Y.Q. Yang, J.Y. Wang, J.P. Zhao, B.-L. Su, Y. Li, Layered polyaniline/graphene film from sandwich-structured polyaniline/graphene/polyaniline nanosheets for high-performance pseudosupercapacitors, J. Mater. Chem. A 2 (2014) 4642–4651.